Electrochimica Acta 512 (2025) 145417

Contents lists available at ScienceDirect

Electrochimica Acta

journal homepage: www.journals.elsevier.com/electrochimica-acta

# Analytical theoretical framework for closed bipolar electrochemical cells under homogeneous molecular catalysis: Implications for electrochemiluminescence applications

Javier López-Asanza [a], Deric Andrade-Alarcón [b], Angela Molina [a,*], Eduardo Laborda [a,*]

[a] Departamento de Química Física, Facultad de Química, Regional Campus of International Excellence "Campus Mare Nostrum", Universidad de Murcia 30100 Murcia, Spain
[b] UCAM-SENS, Universidad Católica San Antonio de Murcia, UCAM HiTech, Avda. Andrés Hernández Ros 1 30107 Murcia, Spain

ARTICLE INFO

*Keywords:*
Two polarized interfaces
Analytical model
Electrogenerated chemiluminiscence
Homogeneous molecular catalysis
Voltammetry

ABSTRACT

A novel analytical framework has been formulated to describe the current-potential-time response in systems with two polarized interfaces where one charge transfer process follows a catalytic mechanism, as found in co-reactant electrochemiluminescence (ECL) systems. The developed theory provides mathematical expressions for electrochemical and ECL signals, concentrations, and interfacial potentials upon the application of a constant potential pulse. Theoretical analysis reveals that the chemical regeneration of the redox reactant within the catalytic cycle has a remarkable impact on the chronoamperometric, voltammetric, and ECL responses, thereby providing means to estimate the catalytic rate constant and to optimize light emission. The system's behaviors are rationalized through the influence of catalysis on the interfacial concentrations and potentials. Also, the primary theoretical predictions have been experimentally validated using the $[Ru(bpy)_3]^{2+}$/oxalate ECL system.

## 1. Introduction

A number of relevant electrochemical systems comprise multiple polarized interfaces (PIs) in series where two or more heterogeneous charge transfers (either electronic or ionic) take place concomitantly: paired electrolysis, closed bipolar cells (cBPCs), solvent polymeric membranes, film-modified electrodes, … [1–7] The charge-balance coupling of the interfacial processes reflects on peculiar behaviours of the electrochemical response [8–12], in contrast with conventional 1PI systems [13].

A chief parameter to be analysed and understood to predict the behaviour of multiple PI cells is the ratio between the maximum current that can flow across each interface (hereafter, the parameter of asymmetry, $\varepsilon$ ) [14,15]. Depending on the $\varepsilon$ -value, the current will be controlled by one or by several charge transfer processes, and the driving force (*i.e.*, the applied potential) will distribute differently between the interfaces. Asymmetric conditions for charge transfer between the interfaces can arise due to different factors. First, the concentration and diffusivity of the electroactive reactant can differ, as well as the interfacial areas. This situation has been examined in previous works for 2PI systems in chronoamperometry and in cyclic voltammetry [1,14,15], pointing out the peculiarities of the 2PI cell response such as the shift of the voltammetric wave with the concentration redox species, and the larger peak-to-peak separation with respect to 1PI systems.

In this work, a mechanistic source of asymmetry will be considered with one of the charge transfers not following a simple E mechanism but a catalytic-type mechanism (see Scheme 1); as a result, the asymmetry parameter $\varepsilon$ is dependent on the catalytic rate constant and on time, in contrast with the case where there are no coupled chemical reactions [14]. Such situation can be found in electrochemiluminiscence (ECL) cells, where a catalytic process typically takes place in the optical compartment [16,17], as well as in parallel paired electrolysis [18]. An analytical theoretical framework will be developed for the comprehensive and insightful study of the above systems under the application of a constant potential pulse, including simple expressions for the current-potential-time and ECL-potential-time responses, the concentration profiles and the interfacial potentials. As will be discussed, the chemical 'boost' of one of the processes through the regeneration in solution of the redox reactant gives rise to a higher capacity for current flow of the corresponding interface. This has a significant impact on the behaviour of the current-potential-time and ECL-time responses, as well as of the interfacial potentials and the redox concentrations, which will

* Corresponding authors.
*E-mail addresses:* amolina@um.es (A. Molina), elaborda@um.es (E. Laborda).

https://doi.org/10.1016/j.electacta.2024.145417
Received 4 September 2024; Accepted 23 November 2024
Available online 25 November 2024

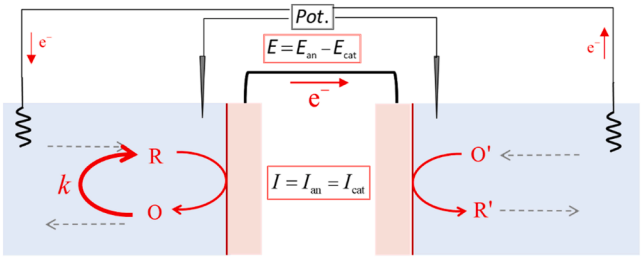


**Scheme 1.** Schematic of the four-electrode cBPC under study.

be investigated in depth and rationalized. Also, procedures for diagnostic and quantitative analysis of the experimental electrochemical and ECL signals will be proposed and applied to the study of the co-reactant ECL system $[Ru(bpy)_3]^{2+}$/oxalate [19,20]

## 2. Materials and methods

Tris(2,2′-bipyridine)ruthenium(II) dichloride ($[Ru(bpy)_3]Cl_2$), potassium nitrate ($KNO_3$, 99 %), hexaammineruthenium(III) chloride ($[Ru(NH_3)_6]Cl_3$), sodium oxalate ($Na_2C_2O_4$), and sulphuric acid 98 % ($H_2SO_4$) were used as reagents. Deionized water from a Milli-Q water purification system with a resistivity of 18.2 MΩ·cm at 25 °C was employed to prepare all the solutions.

The electrochemical and ECL measurements were performed using a four-electrode setup controlled by a BioLogic SP200 potentiostat, in combination with the photodetector system of an SPELEC UV–VIS Instrument 200–900 nm (Metrohm Dropsens). Self-designed cells were used as the cathodic and anodic compartments of the bipolar setup (see Scheme 1), each of them housing a saturated calomel electrode (SCE) as reference electrode and a 0.26 mm-diameter platinum wire as counter (feeder) electrode. The bipolar element that interconnected both compartments consisted of two wire-connected macroelectrodes made of platinum (2 mm-diameter, CH Instruments) in the anodic compartment and glassy carbon (3 mm-diameter, CH Instruments) in the cathodic one. The Pt electrode was anodized prior to the experiments to minimize the interference of oxalate electro-oxidation in the ECL signal [21]. To enhance and streamline the recording of the light signal, the cell employed as ECL compartment (Fig. 1) featured two apertures on opposite sides. Through these, the anodic end of the bipolar element and the optical detector (Reflection Probe VIS-UV, Metrohm Dropsens) were inserted and positioned at an appropriate distance.

## 3. Theory

The boundary value problem (bvp) corresponding to the cBPC shown Scheme 1 when a constant potential pulse, $E$, is applied is given by:

$$\begin{array}{ll} \textit{Anodic compartment} & \textit{Cathodic compartment} \\ \dfrac{\partial c_R(x,t)}{\partial t} = D_{an}\dfrac{\partial^2 c_R(x,t)}{\partial x^2} + k' c_O & \dfrac{\partial c_{O'}(x,t)}{\partial t} = D_{cat}\dfrac{\partial^2 c_{O'}(x,t)}{\partial x^2} \\ \dfrac{\partial c_O(x,t)}{\partial t} = D_{an}\dfrac{\partial^2 c_O(x,t)}{\partial x^2} - k' c_O & \dfrac{\partial c_{R'}(x,t)}{\partial t} = D_{cat}\dfrac{\partial^2 c_{R'}(x,t)}{\partial x^2} \end{array} \quad (1)$$

$$\left.\begin{array}{l} t = 0,\ x \geq 0 \\ t > 0,\ x \to \infty \end{array}\right\} \quad \begin{array}{l} c_R(x,t) = c_R^*,\quad c_{O'}(x,t) = c_{O'}^* \\ c_O(x,t) = 0,\quad c_{R'}(x,t) = 0 \end{array} \quad (2)$$

$t > 0, x = 0$ :

$$\begin{aligned} D_{an}\left(\frac{\partial c_O}{\partial x}\right)_{x=0} &= -D_{an}\left(\frac{\partial c_R}{\partial x}\right)_{x=0} \\ D_{cat}\left(\frac{\partial c_{O'}}{\partial x}\right)_{x=0} &= -D_{cat}\left(\frac{\partial c_{R'}}{\partial x}\right)_{x=0} \\ c_O^s &= e^{\eta_{an}} c_R^s \\ c_{O'}^s &= e^{\eta_{cat}} c_{R'}^s \end{aligned} \quad (3)$$

with $c_i^s$ being the interfacial concentration of species i ( $\equiv O, R, O', R'$) and:

$$\begin{aligned} \eta_{an} &= \frac{F}{RT}\left(E_{an} - E_{O/R}^{0'}\right) \\ \eta_{cat} &= \frac{F}{RT}\left(E_{cat} - E_{O'/R'}^{0'}\right) \end{aligned} \quad (4)$$

where the unknown potential differences at the anodic, $E_{an}$, and cathodic, $E_{cat}$, electrode-solution interfaces are related by:

$$E = E_{an} - E_{cat} \quad (5)$$

and the current across the two interfaces must be equal:

$$I = I_{an} = I_{cat} \quad (6)$$

In order to obtain a solution for this problem, the concentration profiles in the cathodic compartment will be assumed to be equivalent to those obtained for a purely diffusive process, as in the case of non-catalytic reactions in cBPCs. On the other hand, the concentration profiles in the anodic compartment will be supposed to be given by the corresponding expressions in 1PI systems:

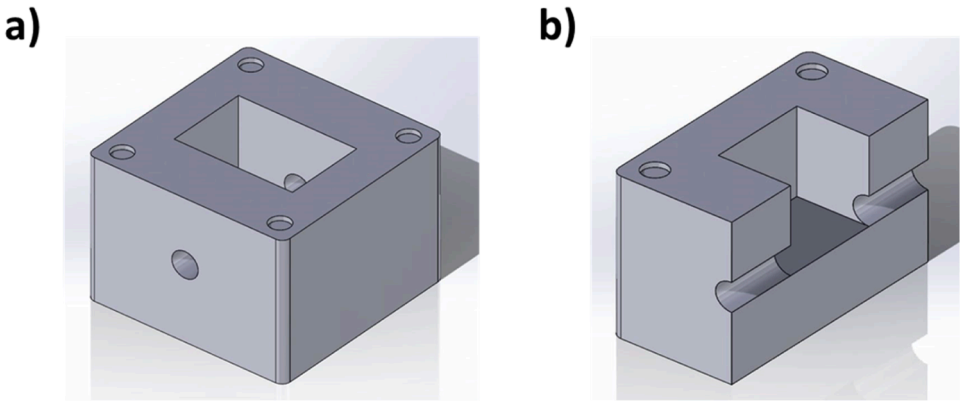


**Fig. 1.** a) General and b) cross-sectional views of the cell employed as anodic compartment where the ECL signal is registered.

*Anodic compartment*

$$c_R = c_R^* - \frac{c_R^* - c_R^s}{2}\left[e^{-x\sqrt{\frac{k'}{D_{an}}}}erfc\left(\frac{x}{2\sqrt{D_{an}t}} - \sqrt{k't}\right) + e^{-x\sqrt{\frac{k'}{D_{an}}}}erfc\left(\frac{x}{2\sqrt{D_{an}t}} + \sqrt{k't}\right)\right]$$

$$c_O = \frac{c_O^s}{2}\left[e^{-x\sqrt{\frac{k'}{D_{an}}}}erfc\left(\frac{x}{2\sqrt{D_{an}t}} - \sqrt{k't}\right) + e^{-x\sqrt{\frac{k'}{D_{an}}}}erfc\left(\frac{x}{2\sqrt{D_{an}t}} + \sqrt{k't}\right)\right] \quad (7)$$

*Cathodic compartment*

$$c_{R'} = c_{R'}^s\, erfc\left(\frac{x}{2\sqrt{D_{cat}t}}\right)$$

$$c_{O'} = c_{O'}^* + \left(c_{O'}^s - c_{O'}^*\right) erfc\left(\frac{x}{2\sqrt{D_{cat}t}}\right)$$

Thus, the current intensity can be approximately expressed using the following relationships:

$$I = FA_{cat}D_{cat}\left(\frac{\partial c_{O'}}{\partial x}\right)_{x=0} = FA_{cat}D_{cat}\left(\frac{c_{O'}^* - c_{O'}^s}{\delta_d(t)}\right) = FA_{cat}D_{cat}\frac{c_{R'}^s}{\delta_d(t)} \quad (8)$$

$$I = FA_{an}D_{an}\left(\frac{\partial c_R}{\partial x}\right)_{x=0} = FA_{an}D_{an}\left(\frac{c_R^* - c_R^s}{\delta_r(t)}\right) = FA_{an}D_{an}\frac{c_O^s}{\delta_r(t)} \quad (9)$$

with:

$$\delta_d(t) = \sqrt{\pi D_{cat}t} \quad (10)$$

$$\delta_r(t) = \sqrt{\frac{D_{an}}{k'}}\,\frac{\sqrt{\pi k't}}{e^{-k't} + \sqrt{\pi k't}\,erf\sqrt{(k't)}} \quad (11)$$

The expression (11) of the thickness of the reaction layer simplifies for values of $kt > 2$:

$$\delta_r(t) = \sqrt{\frac{D_{an}}{k'}} \quad (12)$$

Based on Eqs. (7), (8) and (9), the following expressions for the surface concentrations as a function of the current intensity are derived:

*Anodic compartment*

$$c_R^s = c_R^*\left(1 - \frac{I_N}{\varepsilon(t)}\right)$$

$$c_O^s = c_R^*\frac{I_N}{\varepsilon(t)} \quad (13)$$

*Cathodic compartment*

$$c_{R'}^s = c_{O'}^*\, I_N$$

$$c_{O'}^s = c_{O'}^*(1 - I_N)$$

where

$$I_N = \frac{I}{I_{lc}} \quad (14)$$

with $I_{lc}$ being the maximum current that can flow across the cathodic pole (i.e., the cathodic limiting current)

$$I_{lc} = \frac{FA_{cat}D_{cat}c_{O'}^*}{\delta_d(t)} \quad (15)$$

and

$$\varepsilon(\chi) = \frac{A_{an}D_{an}c_R^*}{A_{cat}D_{cat}c_{O'}^*}\frac{\delta_d(t)}{\delta_r(t)} = \varepsilon_0\left(e^{-\chi} + \sqrt{\pi\chi}\ \mathrm{erf}\left(\sqrt{\chi}\right)\right) \quad (16)$$

$$\chi = k't \quad (17)$$

$$\varepsilon_0 = \frac{A_{an}D_{an}c_R^*}{A_{cat}D_{cat}c_{O'}^*} \quad (18)$$

The expression for the parameter $\varepsilon(\chi)$ can be simplified for values $\chi > 2$ based on Eqs. (10) and (12):

$$\varepsilon(\chi) = \varepsilon_0\sqrt{\pi\chi} \quad (19)$$

Combining the expressions for the surface concentrations (Eqs. (13)) with the Nernst conditions in Eqs. (3), the following expressions for the interfacial potentials of both compartments are obtained:

$$E_{cat} = E_{O'/R'}^{0'} + \frac{RT}{F}\ln\left(\frac{1 - I_N}{I_N}\right)$$

$$E_{an} = E_{O/R}^{0'} + \frac{RT}{F}\ln\left(\frac{I_N}{\varepsilon(\chi) - I_N}\right) \quad (20)$$

Based on Eq. (5) and those for the interfacial potentials (20), the following expression for the potential of the bipolar system as a function of the current is obtained:

$$E = E_{an} - E_{cat} = \Delta E^{0'} + \frac{RT}{F}\ln\left(\frac{I_N^2}{(\varepsilon(\chi) - I_N)(1 - I_N)}\right) \quad (21)$$

with

$$\Delta E^{0'} = E_{O/R}^{0'} - E_{O'/R'}^{0'} \quad (22)$$

Finally, solving the current in Eq. (21) the following expression for the *I-E* curve is obtained:

$$I_N = \frac{(\varepsilon(\chi) + 1)e^{\eta} - \sqrt{(\varepsilon(\chi) - 1)^2e^{2\eta} + 4\,\varepsilon(\chi)\,e^{\eta}}}{2(e^{\eta} - 1)} \quad (23)$$

with

$$\eta = \frac{F(E - \Delta E^{0'})}{RT} \quad (24)$$

From Eq. (21), the expression of the half-wave potential, at which the cell current is half of the limiting value (*i.e.*, $I_N = 1/2$), is also readily derived:

$$E_{1/2} = \Delta E^{0'} - \frac{RT}{F}\ln(2\,\varepsilon(\chi) - 1) \quad (25)$$

as well as the expression of $|E_{3/4} - E_{1/4}|$ related to the steepness of the current-potential curve:

$$|E_{3/4} - E_{1/4}| = \frac{RT}{F} ln\left(27\left(\frac{4\varepsilon(\chi)-1}{4\varepsilon(\chi)-3}\right)\right) \quad (26)$$

### 3.1. ECL theoretical response

Co-reactant ECL mechanisms typically involves high-energy electron transfer reaction between an electrochemically generated species (O in this case) and a co-reactant (S) that yields a light-emitting excited state R* that can undergo radiative relaxation; as a first approach, the following simplified reaction scheme can be considered to describe such process:

$$\begin{array}{l} R \rightleftharpoons O + e^- \\ O \xrightarrow[+S]{k'} R^*(+P) \\ R^* \rightarrow R + h\nu \end{array} \quad (I)$$

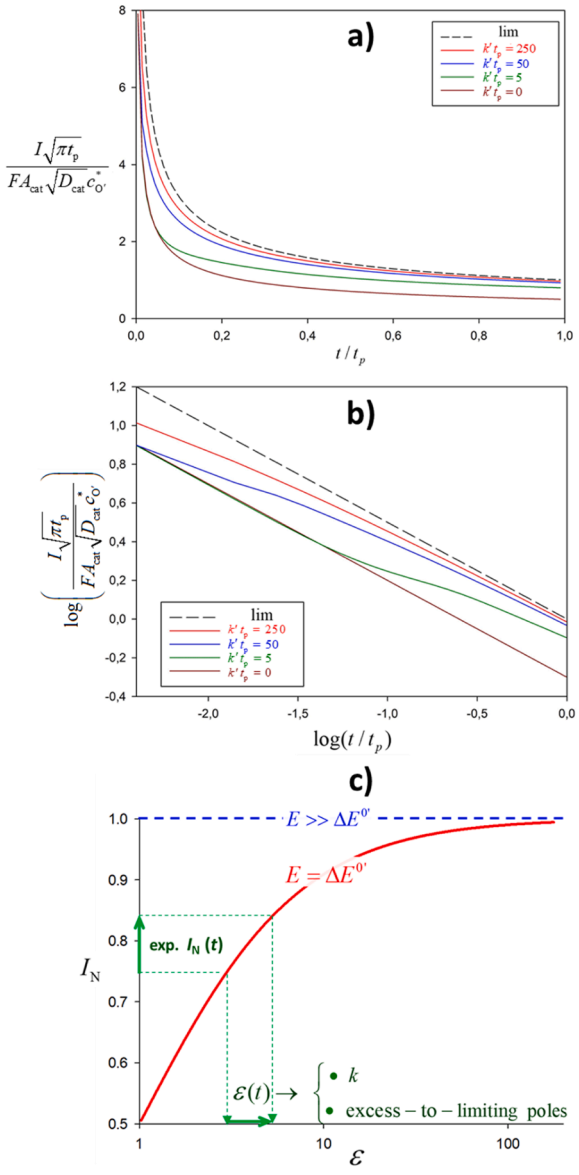


**Fig. 2.** a) Dimensionless chronoamperometry of the cBPC for different values of the catalytic constant, $k'$ (indicated in the legends), b) log-log plot of the chronoamperometric response and c) variation of the normalized current with $\varepsilon$ at $E = \Delta E^{0'}$. $t_p$ corresponds to the total duration of the potential pulse.

Accordingly, the ECL intensity (number of photons emitted *per* second) is expressed by the following equation:

$$I_{ECL} = N_A A_{an} \Phi \int_0^\infty k' c_O(x,t)\, dx \quad (27)$$

where $N_A$ is Avogadro's number and $\Phi$ the quantum yield. From Eq. (27), integrating the concentration profile of the electrogenerated species in the catalytic compartment (Eq. (7)), the following expression is obtained for the ECL intensity:

$$I_{ECL} = \Phi \frac{\sqrt{\pi\chi}\,\mathrm{erf}(\sqrt{\chi})}{e^{-\chi} + \sqrt{\pi\chi}\,\mathrm{erf}\sqrt{\chi}} N_A \frac{I}{F} \quad (28)$$

## 4. Results and discussion

The influence of the catalytic rate constant, on the chronoamperometric response is shown in Fig. 2a considering that the areas, redox concentrations and diffusivities are the same for both charge transfers (*i.e.*, $\varepsilon_0 = 1$); hence, the only source of asymmetry has to do with the occurrence of the coupled catalytic reaction. Within the criterion here considered (Eq. (5)), the global process $R + O' \rightarrow O + R'$ is thermodynamically more favourable as the applied potential $E$ is more positive. Accordingly, the current is negligible at very negative potentials ($I_N(E << \Delta E^{0'}) \rightarrow 0$, see Eq. (5)) and it increases as $E$ is more positive until reaching the limiting value independent of the catalytic kinetics and fully controlled by the diffusion of O' towards the cathodic interface:

$$\lim_{E-\Delta E^{0'}\rightarrow\infty} I_N = I_{N,lim} = \frac{\varepsilon(\chi) + 1 - (\varepsilon(\chi) - 1)}{2} = 1 \quad (29)$$

This limit situation corresponds to the dashed-line curve in Fig. 2a and 2b.

At intermediate potentials (Fig. 2a), a notably interesting chronoamperometric response is observed, which varies with the catalytic rate constant such that an increase in the catalysis rate corresponds to a higher current. In particular, for the value $E = \Delta E^{0'}$ considered in Fig. 2 the current-time response (23) simplifies to:

$$I_N(E = \Delta E^{0'}) = \frac{\varepsilon(\chi)}{1 + \varepsilon(\chi)} \quad (30)$$

Accordingly, in the limit of very small $\chi$ it is fulfilled that $\varepsilon(\chi) \rightarrow 1$ and $I_N \rightarrow 1/2$, while in the other limit of very large $\chi$ it holds that $\varepsilon(\chi) >> 1$ and $I_N \rightarrow 1$. Hence, the response at any intermediate potential and for any chemical kinetics tend to converge to the non-catalytic limiting current. Such transition can be better illustrated via the logarithmic analysis of the chronoamperometric response (Fig. 2b) where a linear Cottrellian relationship is observed at short times (*i.e.*, for small $k't$-values), followed by a non-linear transition towards another Cottrellian regime corresponding to the cathodic limiting current. It is also noteworthy that, despite the first-order EC' mechanism considered at the anodic interface (Scheme 1), a steady-state response is not achieved, which contrasts with the behavior observed in 1PI systems [13]. This is clearly a consequence of the current being limited by the coupled diffusion-controlled process at the cathode.

Taking into account the above, Fig. 2c shows a working curve for the characterization of the chemical kinetics (or of the 2PI cell) based on the variation of the normalized current with $\varepsilon$ for $E = \Delta E^{0'}$. Thus, from the experimental chronoamperometric signal, a set of time-dependent $\varepsilon$-values can be derived from the working curve and, subsequently, from Eq. (16) or (19), the catalytic rate constant (or the limiting-to-excess pole ratio, $\varepsilon_0$) can be determined.

In order to get insights into the origin of the peculiar chronoamperometric behaviour of 2PI systems in the presence of a coupled catalytic reaction, the evolution of the interfacial potentials and interfacial concentrations of the electroactive reactants are analysed in Fig. 3

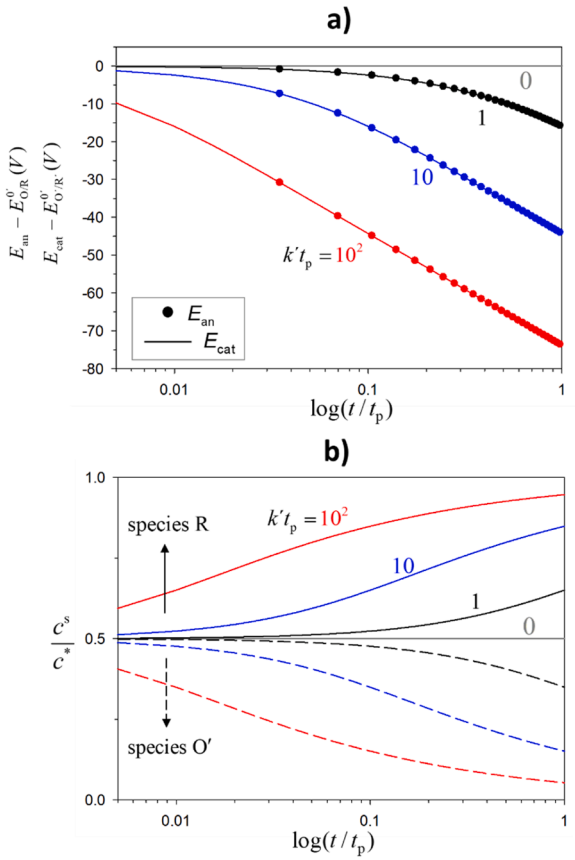


**Fig. 3.** a) Variation of the cathodic and anodic interfacial potentials (Eqs. (20)) and b) the interfacial concentrations of the redox reactants (Eqs.(13)) with time for different values of the catalytic rate constant (indicated on the curves). Other conditions as in Fig. 2.

for the same conditions considered in Fig. 2: $\varepsilon_0 = 1$ and $E = E_{an} - E_{cat} = \Delta E^{0'}$

Both the interfacial potentials and concentrations show time-independent values at short times. In such period, the incidence of the chemical reaction is negligible and the cell behaves equivalently to a 2PI cell where the two charge transfers follow simple E mechanism[14]. As time proceeds, the interfacial potentials and concentrations become time-dependent. Specifically, the two interfacial potentials shift towards more negative values (Fig. 3a), which is related to the non-catalytic cathodic reaction being 'pulled' by the anodic process that is boosted by the catalytic reaction. Obviously, this effect is more apparent as the $k$'-value is larger.

As a result of the above, the interfacial concentration of species O' decreases with time (Fig. 3b) until reaching a null value at long enough times and/or sufficiently fast chemical kinetics. Such situation corresponds to cathodic limiting current conditions, as reflected by the current response (Fig. 2). On the other hand, the interfacial concentration of species R increases with time as the chemical regeneration overcompensates its consumption in the electrode process, the rate of which is limited by the cathodic process. Under the specific conditions considered in Fig. 3 ($E = \Delta E^{0'}$), the concentration changes are mirror-image as can be immediately deduced from Eqs. (13) and (30):

$$c^s_{O'} = c^*_{O'}\frac{1}{1+\varepsilon(\chi)}$$
$$c^s_{R} = c^*_{R}\frac{\varepsilon(\chi)}{1+\varepsilon(\chi)} \quad (31)$$

The time-dependence of the interfacial potentials and concentrations also have an impact on the normal pulse voltammetry response. As shown in Fig. 4a, under the occurrence of the catalytic reaction, the position of the voltammogram shifts with time: the longer the pulse time, the less positive the signal position. This can be parameterized via the half-wave potential, $E_{1/2}$, given by Eq. (25). With respect to the magnitude of the voltammogram, this is not affected by the chemical kinetics under the conditions considered in Fig. 4a since, in all cases, the non-catalyzed cathodic reaction is the current-limiting process (i.e., in all cases $\varepsilon > 1$).

According to Eq. (21), regardless of the $k$'-value, the current-potential curve can be linearized by plotting the applied potential versus $\ln\left(\frac{I_N^2}{(\varepsilon(\chi)-I_N)(1-I_N)}\right)$, such that the intercept value will correspond to $\Delta E^{0'}$ and the slope to $RT/F$, as shown in Fig. 4b. It is worth noting that in conventional one-polarized systems the current-potential response can also be linearized for the E and the first-order catalytic mechanisms with reversible electron transfers, although in 1PI systems the linear relationship holds between $E$ and $\ln\left(\frac{I_N}{1-I_N}\right)$. Such a plot of $E$ vs $\ln\left(\frac{I_N}{1-I_N}\right)$ would not yield a linear trend in 2PI cells except for the specific case $\varepsilon =$

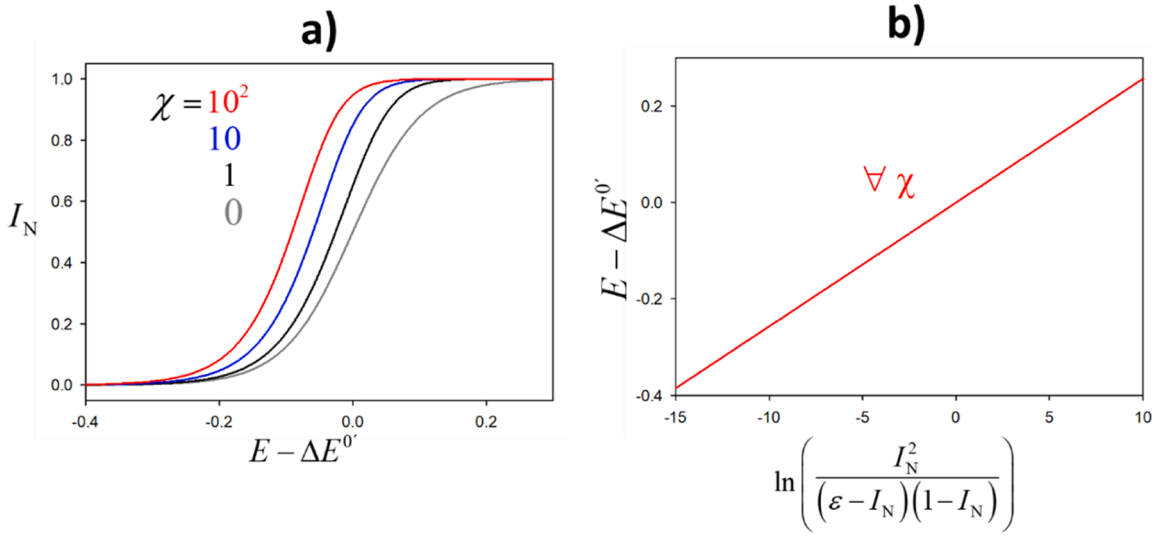


**Fig. 4.** Theoretical a) current–potential (Eqn. (23)) response as a function of the dimensionless parameter $\chi$ and b) the corresponding plots $E$ *vs* $\ln\left(\frac{I_N^2}{(\varepsilon(\chi)-I_N)(1-I_N)}\right)$.

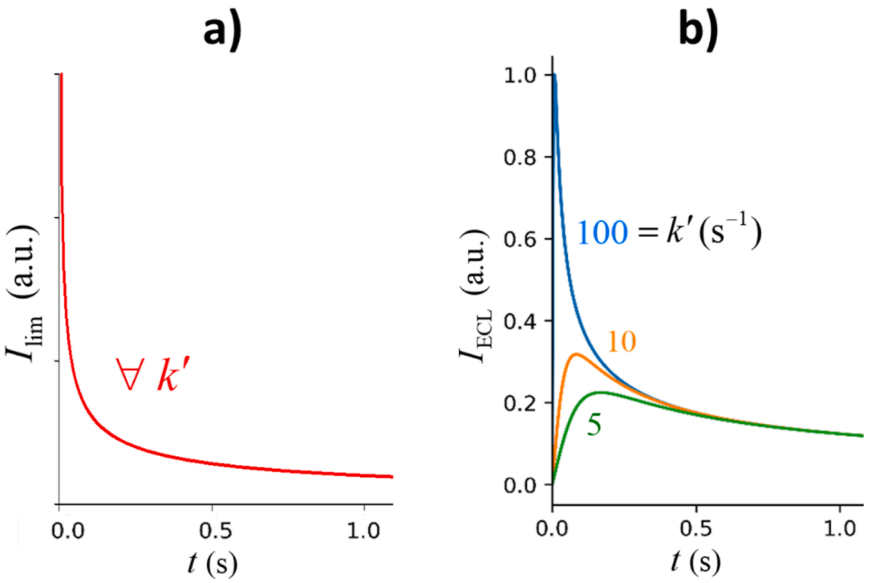


**Fig. 5.** Theoretical a) current-time response under limiting current conditions (Eq. (15)) and b) ECL-time signal (Eq. (28)) for different values of *k'* (indicated on the curves).

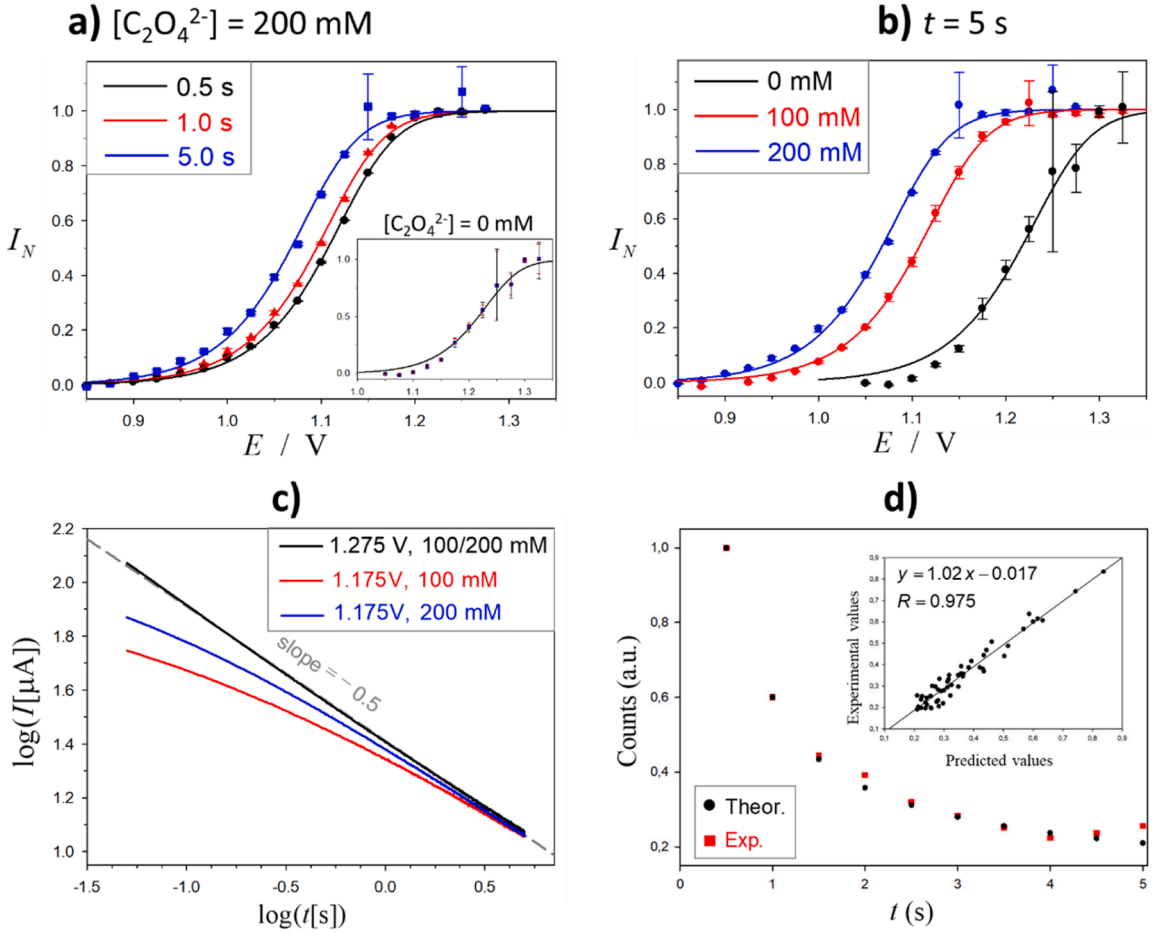


**Fig. 6.** **a**-b) Experimental (points) and best-fit theoretical (lines) current-potential curves at different pulse times or oxalate concentrations (indicated on the graphs); error bars correspond to the standard deviation of three experiments. c) Log-log plot of the current-time response for $E = 1.275$ V (black line) and 1.175 V (red and blue lines) at different oxalate concentrations (indicated in the legend). d) Experimental and theoretical ECL signals (counts at an integration time of 0.5 s) under limiting current conditions; *inset*: correlation plot between experimental and theoretical ECL signals for five experiments. Cathodic solution: 3 mM $[Ru(NH_3)_6]Cl_3$, 0.4 M KCl; anodic solution: 1 mM $[Ru(bpy)_3]Cl_2$, x mM $NaC_2O_4$, 0.1 M KCl, phosphate buffer (pH = 7).

1, where it would result in a slope of $2RT/F$.

Fig. 5 shows the comparison between the electrochemical and the ECL signals for a chronoamperometric experiment under most typical working conditions of limiting current (*i.e.*, $E >> \Delta E^{0'}$). As mentioned above, since the current is controlled by the cathodic pole, the current-time signal shows a Cottrellian time-dependence and it is insensitive to the chemical rate constant. On the other hand, the ECL-time curve does show a marked dependence on the $k$'-value. Thus, as shown in Fig. 5b, the ECL signal shows a non-monotonous behaviour so that it takes a null value at very short times where the effects of the chemical kinetics is obviously negligible; subsequently, the ECL signal increases with time until reaching a maximum, beyond which there is a Cottrellian decay due to that the ECL is proportional to the rate of electrogeneration of the reactant of the luminescent process (i.e., species O), which is limited by the non-catalyzed reaction. Both limits can be readily deduced from Eq. (28) by making either $\chi \to 0$ (very short times) or $\chi >> 1$:

$$\lim_{\chi \to 0} I_{ECL} = 0 \tag{32}$$

$$\lim_{\chi >> 1} I_{ECL} = \Phi N_A \frac{I}{F} = \text{constant} \times I \tag{33}$$

The behaviours and results predicted by the analytical model have been investigated experimentally with the cBPC detailed in Section 2, with the monoelectronic electro-reduction of $[Ru(NH_3)_6]^{3+}$ taking place at the cathodic end of the bipolar element:

$$[Ru(NH_3)_6]^{3+} + e^- \rightleftarrows [Ru(NH_3)_6]^{2+} \quad \textit{Cathodic pole} \tag{II}$$

and the electro-oxidation of $[Ru(bpy)_3]^{2+}$ at the anodic pole

$$[Ru(bpy)_3]^{2+} - e^- \rightleftarrows [Ru(bpy)_3]^{3+} \quad \textit{Anodic pole} \tag{III}$$

that, in presence of oxalate, triggers the co-reactant ECL mechanism described by [19]:

$$\begin{gathered}
[Ru(bpy)_3]^{3+} + C_2O_4^{2-} \xrightarrow[rds]{k} [Ru(bpy)_3]^{2+} + C_2O_4^{\bullet -} \quad (a) \\
C_2O_4^{\bullet -} \rightarrow CO_2^{\bullet -} + CO_2 \quad (b) \\
[Ru(bpy)_3]^{3+} + CO_2^{\bullet -} \rightarrow [Ru(bpy)_3]^{2+*} + CO_2 \quad (c) \\
[Ru(bpy)_3]^{2+} + CO_2^{\bullet -} \rightarrow [Ru(bpy)_3]^{+} + CO_2 \quad (d) \\
[Ru(bpy)_3]^{3+} + [Ru(bpy)_3]^{+} \rightarrow [Ru(bpy)_3]^{2+*} + [Ru(bpy)_3]^{2+} \quad (e) \\
[Ru(bpy)_3]^{2+*} \rightarrow [Ru(bpy)_3]^{2+} + h\nu \quad (f)
\end{gathered} \tag{IV}$$

In excess of oxalate in solution and neglecting the effect of steps IVd and IVe, the rate of regeneration of $[Ru(bpy)_3]^{3+}$ by scheme (IV) can be tackled according to the pseudofirst-order catalytic mechanism considered in the theoretical framework (see Supporting Information), $2[Ru(bpy)_3]^{3+} \rightarrow^{k'_{+C_2O_4^{2-}}} 2[Ru(bpy)_3]^{2+} + h\nu$, with an apparent homogenous rate constant $k' = 2k[C_2O_4^{2-}]$.

Figs. 6a and 6b show the experimental current-potential curves (points) obtained at different pulse durations (0.5, 1 and 5 s) and different concentrations of oxalate (0, 100 and 200 mM) together with the best-fit theoretical curves (solid lines; Eq. (23)). As can be observed, in all the conditions considered a very good agreement between the experimental and theoretical results is attained. Thus, the influence of the pseudo-first order kinetics and the duration of the potential pulse on the current-potential curves follow the trends pointed out by the model: The enhancement of the catalytic contribution via the increase of $k$' (through the increment of the oxalate concentration) and of the pulse duration leads to voltammetric signals situated at less positive potentials, as corresponds to larger $\varepsilon$-values (see Fig. 4). This contrasts with the results obtained in the absence of oxalate (inset in Fig. 6a) where the position of the current-potential curve is independent of the duration of the potential pulse. The analysis of the shift of the half-wave potential with Eq. (25) yielded a value of the apparent homogeneous rate constant of $k = (15 \pm 3) \times 10^3\ M^{-1}s^{-1}$, which is not significantly different from the value obtained from the steady state limiting current recorded in the anodic compartment with a conventional three-electrode setup ($k = (8.9 \pm 0.5) \times 10^3\ M^{-1}s^{-1}$, see Supporting Information).

The striking chronoamperometric behaviour discussed in Fig. 2 has also been observed experimentally. As shown in Fig. 6c, a linear relationship between $\log(I)$ and $\log(t)$ with a slope close to $-0.5$ is obtained under limiting current conditions ($E = 1.275$ V, black line). When a less positive potential $E = 1.175$ V is applied, the linearity of the log-log plot is lost at short times (red and blue lines) and, as time proceeds, it is gradually recovered in such a way that the experimental current approaches the limiting value. As predicted theoretically, such transition takes place at shorter times as $k$' is larger, that is, as the oxalate concentration is higher (compare red and blue lines).

Finally, the experimental ECL signal was also registered under limiting current conditions (red squares in Fig. 6d). A monotonous decay of the number of counts with time is found, with satisfactory agreement between the experimental trend and the theoretical predictions with Eq. (33) (see inset in Fig. 6d), pointing out that, under the conditions of the study, the magnitude of the ECL signal is controlled by the diffusion of $[Ru(NH_3)_6]^{3+}$ to the cathodic pole.

## 5. Conclusions

A novel analytical theory has been developed for the current-potential-time response of two polarized interface systems where one of the charge transfers follows a first-order catalytic process. Mathematical expressions have been presented for the electrochemical signals, as well as for the concentration and interfacial potentials. The analysis of the latter shows that, as a consequence of the chemical regeneration of the redox reactant in the catalytic cycle, the current flow that can be delivered by the catalyzed compartment is enhanced. As a result, the interfacial concentrations of the reactant of the non-catalyzed reaction gradually depletes at the interface, even at potentials that initially do not correspond to limiting current conditions. This phenomenon has striking effects on the current-potential-time response. First, a transition towards the limiting current is achieved, not by increasing the applied potential, but by lengthening the duration of the perturbation. Second, the position of the voltammetric signal is time-dependent, unlike in the absence of catalysis, in such a way that the current-potential response develops 'earlier' as the time-scale of the experiment is longer. Hence, the quantitative analysis of the time-dependence of the chronoamperometric signal and of the half-wave potential can be used for the estimation of the catalytic rate constant.

With regard to the ECL-time response, under the most common working conditions of chronoamperometry at potentials of maximum current, chronoamperometry is not useful for the study of the chemical reaction since this is insensitive to it. On the other hand, the ECL signal shows a maximum at intermediate kinetics that appears earlier and increases with the catalytic rate constant.

All the 'peculiar' chronoamperometric and voltammetric features predicted by the theory have been verified experimentally, both for the electrochemical and ECL signals, through the study of the $[Ru(bpy)_3]^{2+}$/oxalate ECL system.

## CRediT authorship contribution statement

**Javier López-Asanza:** Formal analysis, Investigation, Software. **Deric Andrade-Alarcón:** Investigation, Methodology. **Angela Molina:** Conceptualization, Investigation, Supervision, Writing – original draft, Writing – review & editing. **Eduardo Laborda:** Conceptualization, Funding acquisition, Supervision, Writing – original draft.

## Declaration of competing interest

The authors declare that they have no known competing financial interests or personal relationships that could have appeared to influence the work reported in this paper.

## Acknowledgements

The Authors sincerely thank Prof. F. Javier del Campo and Dr. R.K. Reddy Gajjala (BCMaterials) for their advice and guidance for the experimental measurements. The Authors also thank the funding provided by Ministerio de Ciencia e Innovación (PID2022–136568NB-I00), as well as by MCIN/AEI/10.13039/501100011033 and the European Union "NextGenerationEU"/PRTR" through the project TED2021–130334B-I00.

## Supplementary materials

Supplementary material associated with this article can be found, in the online version, at doi:10.1016/j.electacta.2024.145417.

## Data availability

Data will be made available on request.

## References

[1] A.A. Stewart, J.A. Campbell, H.H. Girault, M. Edddowes, Cyclic voltammetry for electron transfer reactions at liquid/liquid interfaces, Berichte Der Bunsengesellschaft Für Physikalische Chemie 94 (1990) 83–87, https://doi.org/10.1002/bbpc.19900940117.

[2] Z. Samec, V. Mareček, J. Weber, Charge transfer between two immiscible electrolyte solutions, J. Electroanal. Chem. Interfacial. Electrochem. 103 (1979) 11–18, https://doi.org/10.1016/S0022-0728(79)80475-1.

[3] S. Ulmeanu, H.J. Lee, D.J. Fermin, H.H. Girault, Y. Shao, Voltammetry at a liquid–liquid interface supported on a metallic electrode, Electrochem. Commun. 3 (2001) 219–223, https://doi.org/10.1016/S1388-2481(01)00138-2.

[4] J. González, E. Laborda, A. Molina, Analytical modelling of electron-coupled ion transfers with immobilized vs soluble redox transducer at thick film-modified electrodes, Electroanalysis. 33 (2021) 2267–2277, https://doi.org/10.1002/elan.202100234.

[5] M. Zhou, S. Gan, L. Zhong, X. Dong, J. Ulstrup, D. Han, L. Niu, Improvement in the assessment of direct and facilitated ion transfers by electrochemically induced redox transformations of common molecular probes, Phys. Chem. Chem. Phys. 14 (2012) 3659, https://doi.org/10.1039/c2cp23184k.

[6] B. Nagar, W.O. Silva, H.H. Girault, Voltammetry in two-electrode mode for rapid electrochemical screening using a fully printed and flexible multiplexer sensor, ChemElectroChem. 8 (2021) 3700–3706, https://doi.org/10.1002/celc.202100477.

[7] F. Marken, A.J. Cresswell, S.D. Bull, Recent advances in paired electrosynthesis, Chem. Record 21 (2021) 2585–2600, https://doi.org/10.1002/tcr.202100047.

[8] D. Plana, F.G.E. Jones, R.A.W. Dryfe, The voltammetric response of bipolar cells: reversible electron transfer, J. Electroanalyt. Chem. 646 (2010) 107–113, https://doi.org/10.1016/j.jelechem.2010.03.020.

[9] J.P. Guerrette, S.M. Oja, B. Zhang, Coupled electrochemical reactions at bipolar microelectrodes and nanoelectrodes, Anal. Chem. 84 (2012) 1609–1616, https://doi.org/10.1021/ac2028672.

[10] J. Zhang, W. Yu, X. Jiang, Y. Gao, G. Peng, Alternate reporting surfaces in closed bipolar electrode system: a strategy forelectrochemiluminescence sensing of both redox processes, J. Electroanalyt. Chem. 878 (2020) 114705, https://doi.org/10.1016/j.jelechem.2020.114705.

[11] J.D. Zhang, W.W. Zhao, J.J. Xu, H.Y. Chen, Electrochemical behaviors in closed bipolar system with three-electrode driving mode, J. Electroanalyt. Chem. 781 (2016) 56–61, https://doi.org/10.1016/j.jelechem.2016.10.017.

[12] H. Hotta, N. Akagi, T. Sugihara, S. Ichikawa, T. Osakai, Electron-conductor separating oil-water (ECSOW) system: a new strategy for characterizing electron-transfer processes at the oil/water interface, Electrochem. commun. 4 (2002) 472–477, https://doi.org/10.1016/S1388-2481(02)00343-0.

[13] Á. Molina, J. González, Pulse voltammetry in physical electrochemistry and electroanalysis, Springer International Publishing, Cham, 2016, https://doi.org/10.1007/978-3-319-21251-7.

[14] E. Laborda, J. López-Asanza, A. Molina, Theoretical framework and guidelines for the cyclic voltammetry of closed bipolar cells, Anal. Chem. 95 (2023) 17311–17317, https://doi.org/10.1021/acs.analchem.3c03480.

[15] E. Laborda, A. Molina, Coupled electron transfer reactions in closed bipolar cells: the impact of asymmetric mass transport, Curr. Opin. Electrochem. 39 (2023) 101287, https://doi.org/10.1016/j.coelec.2023.101287.

[16] K.L. Rahn, R.K. Anand, Recent advancements in bipolar electrochemical methods of analysis, Anal. Chem. 93 (2021) 103–123, https://doi.org/10.1021/acs.analchem.0c04524.

[17] T. Iwama, M. Komatsu, K.Y. Inoue, H. Shiku, Detection and 2d imaging of dopamine distribution using a closed bipolar electrode system by applying a cathodic luminophore, ChemElectroChem. 8 (2021) 3492–3498, https://doi.org/10.1002/celc.202100675.

[18] X. Zhang, Z. Li, H. Chen, C. Shen, H. Wu, K. Dong, Pairing electrocarboxylation of unsaturated bonds with oxidative transformation of alcohol and amine, ChemSusChem. 16 (2023) e202300807, https://doi.org/10.1002/cssc.202300807.

[19] F. Kanoufi, A.J. Bard, Electrogenerated chemiluminescence. 65. An investigation of the oxidation of oxalate by tris(polypyridine) ruthenium complexes and the effect of the electrochemical steps on the emission intensity, J. Physic. Chem. B 103 (1999) 10469–10480, https://doi.org/10.1021/jp992368s.

[20] L. Bouffier, D. Zigah, N. Sojic, A. Kuhn, Bipolar (Bio)electroanalysis, Ann. Rev. Analytic. Chem. 14 (2021) 65–86, https://doi.org/10.1146/annurev-anchem-090820-093307.

[21] F.C. Anson, F.A. Schultz, Effect of adsorption and electrode oxidation on the oxidation of oxalic acid at platinum electrodes, Anal. Chem. 35 (1963) 1114–1116, https://doi.org/10.1021/ac60202a045.